nature photonics

LETTERS

https://doi.org/10.1038/s41566-020-0619-8

Check for updates

Test of general relativity by a pair of transportable optical lattice clocks

Masao Takamoto[1,2], Ichiro Ushijima[3], Noriaki Ohmae[1,2], Toshihiro Yahagi[4], Kensuke Kokado[4], Hisaaki Shinkai[5] and Hidetoshi Katori[1,2,3]✉

A clock at a higher altitude ticks faster than one at a lower altitude, in accordance with Einstein's theory of general relativity. The outstanding stability and accuracy of optical clocks, at 10^{-18} levels[1–5], allows height differences[6] of a centimetre to be measured. However, such state-of-the-art clocks have been demonstrated only in well-conditioned laboratories. Here, we demonstrate an 18-digit-precision frequency comparison in a broadcasting tower, Tokyo Skytree, by developing transportable optical lattice clocks. The tower provides the clocks with adverse conditions to test the robustness and a 450 m height difference to test the gravitational redshift at $(1.4 \pm 9.1) \times 10^{-5}$. The result improves ground-based clock comparisons[7–9] by an order of magnitude and is comparable with space experiments[10,11]. Our demonstration shows that optical clocks resolving centimetres are technically ready for field applications, such as monitoring spatiotemporal changes of geopotentials caused by active volcanoes or crustal deformation[12] and for defining the geoid[13,14], which will have an immense impact on future society.

Einstein formulated general relativity (GR) as the theory of gravity in 1915, in which he explained the origin of gravity is the curvature of space and time. Over the century since then, alternative theories of gravity have been proposed, and they have been tested in many ways[15]. Although GR is believed to be the best theory of gravity, there are aspects that are not completely satisfactory. First, although special relativity has been integrated with quantum theory as quantum field theory, GR is not yet unified, preventing a single ultimate theory. Second, the current standard cosmological model based on GR has to introduce unknown 'dark energy' to explain the accelerating Universe[16]. Plausible solutions to the 'dark energy' problem are to throw away the cosmological principle (a homogeneous and isotropic Universe) or to modify GR. Thus, the precise measurement of the validity of GR is an important step towards understanding fundamental physics, even in the classical regime.

GR predicts the dilation of time in a deeper gravitational potential; this is referred to as gravitational redshift. The gravitational redshift between clocks ($\Delta\nu = \nu_2 - \nu_1$) located at positions 1 and 2 is given by their gravitational potential difference $\Delta U = U_2 - U_1$ as

$$\frac{\Delta\nu}{\nu_1} = (1+\alpha)\frac{\Delta U}{c^2} \quad (1)$$

to first order of ΔU, where $\nu_{1(2)}$ is the clock frequency at location 1 (2), c is the speed of light and α denotes the violation from GR ($\alpha = 0$ for GR). The measurement of α at different locations serves as a test of local position invariance (LPI), which describes the result of a non-local gravitational experiment being independent of place and time, which is at the heart of Einstein's equivalence principle, the starting principle of GR.

The first redshift measurement was carried out in the series of Pound–Rebka–Snider experiments[7] in the early 1960s, in which they obtained $|\alpha| < \mathcal{O}(10^{-2})$ with a height difference of $\Delta h = 23$ m. Later, the Gravity Probe A mission[17] obtained $|\alpha| \approx 1.4 \times 10^{-4}$ using a hydrogen maser in a spacecraft launched to $\Delta h = 10{,}000$ km. Recently, using two Galileo satellites that accidentally took elliptic orbits with a height difference of $\Delta h \approx 8{,}500$ km, new constraints were reported as $\alpha = (0.19 \pm 2.48) \times 10^{-5}$ (ref. [10]) and $\alpha = (4.5 \pm 3.1) \times 10^{-5}$ (ref. [11]). The uncertainty of α is mainly given by $\frac{c^2}{\Delta U}\frac{\delta\nu}{\nu_1}$, suggesting that accurate frequency measurement of clocks ($u_c = \delta\nu/\nu_1$) is at the heart of the endeavour, in particular, for ground experiments with Δh less than a kilometre, as ΔU is nearly four orders of magnitude smaller than the space experiments. A comparison of optical lattice clocks at RIKEN and The University of Tokyo[8] with $\Delta h \approx 15$ m has so far demonstrated $\alpha = (2.9 \pm 3.6) \times 10^{-3}$, limited by $u_c = 5.7 \times 10^{-18}$. Constraining α to better than 10^{-3} on the ground has remained uninvestigated, as it requires outstanding clock accuracy or height differences.

Transportable optical clocks with uncertainties below 10^{-16} (refs. [18–20]) and laboratory-based clocks with uncertainties of 10^{-18} (refs. [1–3,5]) or below[4] offer new possibilities for testing fundamental physics on the ground, for example, a test of Lorentz symmetry[21] or a search for dark matter[22–27]. The Physikalisch-Technische Bundesanstalt (PTB) and Istituto Nazionale di Ricerca Metrologica (INRiM) team has reported $\alpha \approx 10^{-2}$ by comparing a transportable clock in the middle of a mountain and a laboratory clock, with $\Delta h \approx 1{,}000$ m (ref. [9]). Here, we demonstrate a test of the gravitational redshift of $\alpha = (1.4 \pm 9.1) \times 10^{-5}$ by developing a pair of transportable optical lattice clocks and operating them with a height difference of $\Delta h \approx 450$ m at Tokyo Skytree.

To operate Sr-based optical lattice clocks at 10^{-18} uncertainty, reducing the blackbody radiation (BBR) shifts[1–3] and the higher-order light shifts[28,29] is of prime concern. Applying a small-sized BBR shield as depicted in Fig. 1a, the ambient temperature in the spectroscopy region is controlled at 245 K by a four-stage Peltier cooler. In addition, we reduce the total lattice light shift to 1×10^{-18} by tuning the lattice laser to frequency $\nu_L = 368{,}554{,}470.4 \pm 0.2$ MHz, with polarization parallel to the bias magnetic field (Fig. 1a), and by setting the lattice depth to $81E_R$, where E_R is the lattice photon recoil energy[29], compensating the multipolar- and hyperpolarizability-induced light shift with the electric-dipole light shift[28]. To

[1]Quantum Metrology Laboratory, RIKEN, Wako, Saitama, Japan. [2]Space-Time Engineering Research Team, RIKEN, Wako, Saitama, Japan. [3]Department of Applied Physics, Graduate School of Engineering, The University of Tokyo, Bunkyo-ku, Tokyo, Japan. [4]Geospatial Information Authority of Japan, Tsukuba, Ibaraki, Japan. [5]Osaka Institute of Technology, Kitayama, Hirakata, Osaka, Japan. ✉e-mail: katori@amo.t.u-tokyo.ac.jp

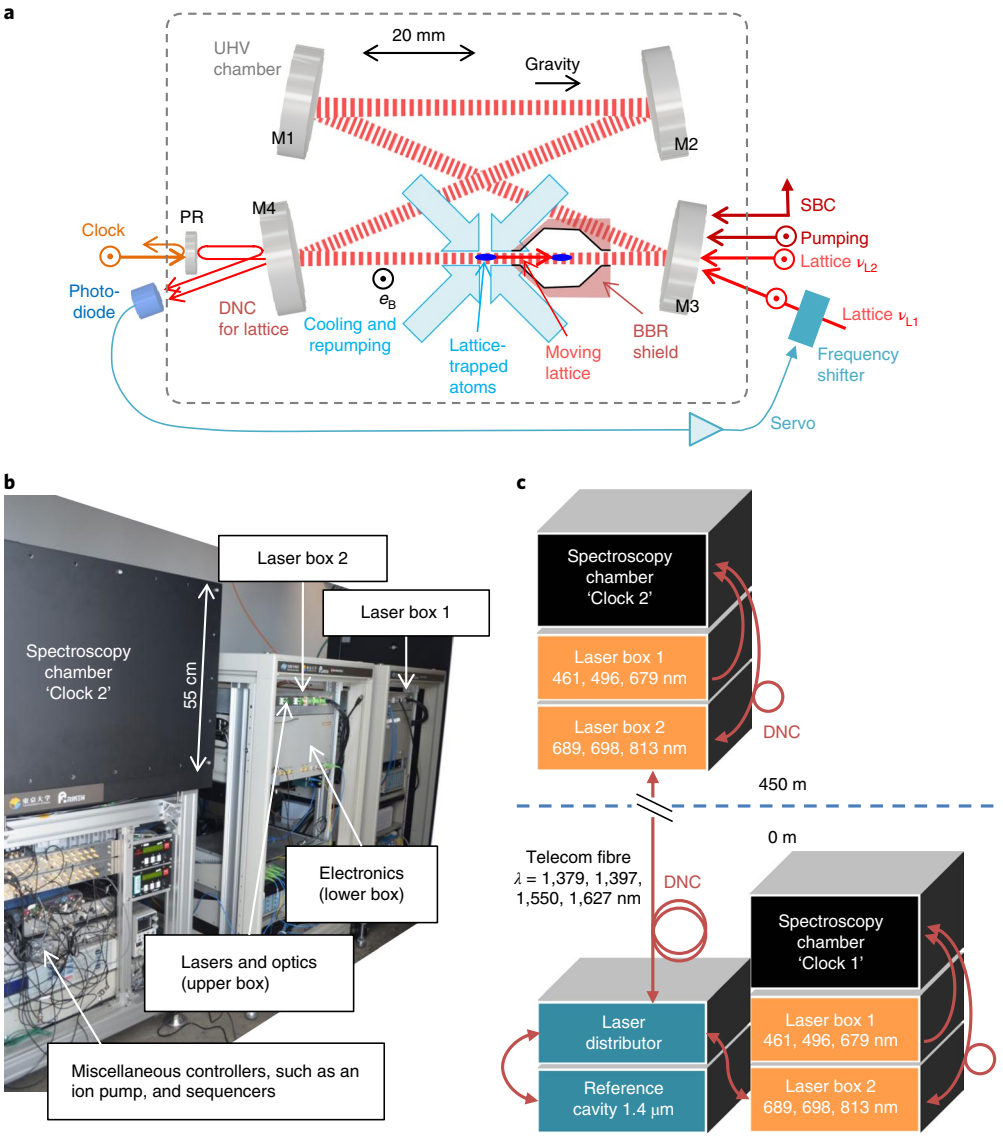

Fig. 1 | Transportable optical lattice clocks. a, Schematic of a clock spectroscopy block installed inside an ultrahigh-vacuum (UHV) chamber. Magneto-optically trapped (MOT) ultracold ^{87}Sr atoms are loaded into a one-dimensional (1D) optical lattice that is formed inside a power-buildup ring cavity consisting of four mirrors (M1–M4). A partial reflector (PR) set 10 mm behind M4 provides a reference surface for the Doppler noise cancellation (DNC). Atoms are transported into an 18-mm-long BBR shield with two apertures of 1 mm diameter by a moving lattice detuned $\Delta\nu_L = \nu_{L2} - \nu_{L1}$ within the cavity linewidth. Polarizations of the clock, pumping and lattice lasers are parallel to the quantization axis $\mathbf{e}_B$ defined by a bias magnetic field of 66 μT, while that of the sideband cooling (SBC) laser is perpendicular to $\mathbf{e}_B$. **b**, A clock system installed in an observatory floor at 450 m in Tokyo Skytree. The physics package for spectroscopy is surrounded by μ-metal shielding. 'Laser boxes' 1 and 2 with outer dimensions of 44(*W*) × 30(*H*) × 64(*D*) cm^3, which include lasers and optics in the upper side and their control electronics in the lower side, are mounted on 19-inch racks. **c**, Two identical clocks are set with a height difference of 450 m. On the ground floor, a clock laser is locked to a reference cavity at 1,397 nm with an instability of 1×10^{-15} at 1 s and is delivered by Doppler-noise-cancelled (DNC) telecom fibres. A 'laser distributor' delivers the sub-harmonics of the clock laser, the second-stage cooling (1,379 nm) and optical lattice (1,627 nm) lasers that are stabilized to a transfer cavity.

accommodate both the well-defined ambient temperature and lattice intensity, we install a ring cavity to transport the atoms into the BBR shield, where the cavity linewidth of ~6 MHz allows transporting atoms by detuning the counter-propagating-laser frequencies $\Delta\nu_L = \nu_{L2} - \nu_{L1}$. The BBR shield also protects lattice-trapped atoms from colliding with the thermal Sr beam from the oven.

The physics package for the clock spectroscopy is set inside a magnetic shield box with a side length of ~60 cm (Fig. 1b) and is operated by two laser boxes (labelled 1 and 2, Fig. 1c). Laser box 1 includes cooling (461 nm, 496 nm) and repumping (679 nm) lasers stabilized via a wavelength meter to within a few MHz. Laser box 2 includes lasers used for cooling on the spin-forbidden transition ($\lambda_1 = 689$ nm), clock spectroscopy ($\lambda_2 = 698$ nm) and the optical lattice ($\lambda_3 = 813$ nm), which require high frequency stabilities. They are phase-stabilized to the second harmonics of corresponding infrared lasers with $2\lambda_1 = 1{,}379$ nm, $2\lambda_2 = 1{,}397$ nm and $2\lambda_3 = 1{,}627$ nm, which are conveniently sent via telecom fibres so as to share stable lasers between the two clocks. On the ground floor, we set a clock laser at $2\lambda_2$ with an instability of 1×10^{-15} at 1 s. A laser distributor box generates frequency-stabilized lasers at $2\lambda_1$ and $2\lambda_3$ using a transfer cavity that is monitored by the clock laser $2\lambda_2$. This distributor box also delivers a radiofrequency (RF) reference at 20 MHz

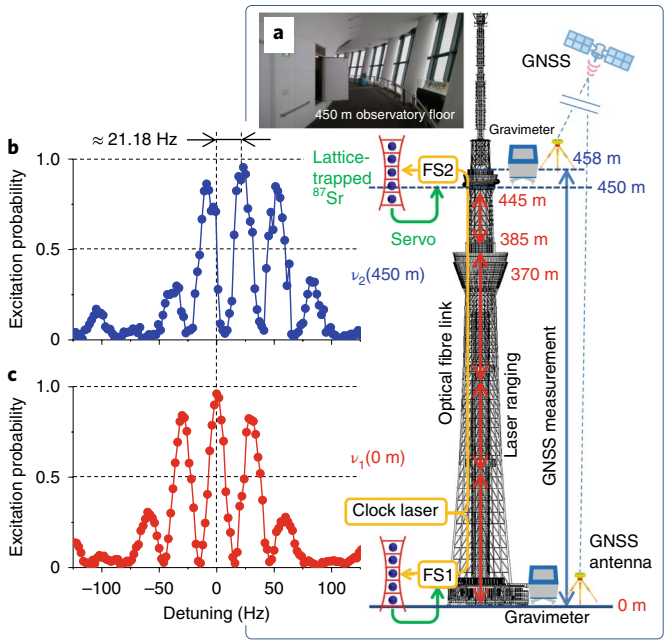

Fig. 2 | Gravitational potential differences investigated by three different methods of chronometric levelling, laser ranging and GNSS complemented by spirit levelling and a gravimeter. a, An upper clock set in a 7-m^2-large room in the observatory floor, as shown in Fig. 1b, is fibre-linked to the other clock on the ground floor. GNSS antennas are set on the 458 m floor and on the ground. The height differences between the antennas and clocks are measured by spirit levelling. Laser ranging is performed in four separate segments as indicated by red arrows. We measure the gravitational accelerations g_0 and g_{450} at 0 m and at the 450 m floor, respectively, and apply the average value $\bar{g} = \frac{g_0+g_{450}}{2}$. **b**,**c**, Ramsey spectra measured in the observatory floor (**b**, blue circles) and the ground floor (**c**, red circles) show the gravitational redshift of ~21.18 Hz.

generated by a Rb clock (with an uncertainty of ~10^{-10}) and a timing signal to operate the clocks; both are sent by amplitude modulation of a carrier at $\lambda_4 = 1{,}550$ nm. These four infrared lasers are mixed by wavelength division multiplexing modules and sent to the two clocks by telecom fibres, where we install Doppler noise cancellers with a servo bandwidth of 10 kHz.

While running the clocks, the geopotential difference between them is investigated by means of the Global Navigation Satellite System (GNSS) and laser ranging complemented by spirit levelling and gravity measurements (Fig. 2a). The height of the core pillar of the tower from 0 m to 370 m and the height from 385 m to 445 m, which covers 94% of the total height difference Δh, is continuously monitored by laser ranging. The remaining 25 m is intermittently measured by laser ranging and spirit levelling (see Methods). Figure 2b,c shows the Ramsey spectra measured on the observatory floor and on the ground floor, respectively, with a pulse duration of 11 ms and a free evolution time of 20 ms. The frequency shift of $\Delta\nu = \nu_2 - \nu_1 \approx 21.18$ Hz corresponds to a gravitational redshift of the clock frequency ($\nu_1 \approx 429.228$ THz) for a height difference of ~450 m. The clock laser frequencies ν_1 and ν_2 are stabilized to the respective Ramsey spectra with a free-evolution time of 40 ms using frequency shifters (FS1 and FS2). By synchronously interrogating the clock transitions, we reduce the Dick effect[8,30], allowing the Allan deviation to improve from 1×10^{-15} at 1 s to 5×10^{-18} after 5×10^4 s (Supplementary Fig. 1b). To reduce uncertainties for the gravitational redshift, we operate the two clocks with the same experimental conditions to reject some systematics, as described in the Methods.

Figure 3 summarizes the geopotential measurements carried out by the clocks, GNSS, laser ranging and gravimeter. We conducted GNSS measurements for five days in October 2018 to obtain $\Delta h = 452.650 \pm 0.039$ m. This agrees with the simultaneous laser ranging value of $\Delta h = 452.631 \pm 0.013$ m within 1σ uncertainty, validating the consistency of the height measurements. The laser ranging continuously monitors the long-term height variation of the tower corresponding to a temperature variation of 10 °C. Figure 3b presents 11 measurements taken to determine the gravitational redshift of $\Delta\nu(\text{Skytree})/\nu_1 = (49{,}337.8 \pm 4.0(\text{sys}) \pm 1.5(\text{stat})) \times 10^{-18}$. After the measurements at Skytree, we transported the system back to RIKEN and compared the two clocks at the same height (Fig. 3d). The measured fractional beat note $\Delta\nu(\text{RIKEN})/\nu_1 = (-0.3 \pm 3.5(\text{sys}) \pm 3.1(\text{stat})) \times 10^{-18}$, as shown in Fig. 3c, confirms the reproducibility of the clocks. Table 1 presents a summary of the height and frequency measurements. During the measurement period 'modified Julian date' (MJD) 58,571–58,577, the gravitational redshift is observed to be $\Delta\nu/\nu_1 = (49{,}337.8 \pm 4.3) \times 10^{-18}$ as mentioned above, while the gravitational potential difference measured by laser ranging gives $\bar{g}\Delta h/c^2 = (49{,}337.1 \pm 1.4) \times 10^{-18}$ with height difference $\Delta h = 452.596(13)$ m and gravitational acceleration $\bar{g} = 9.797248(24)\,\text{m s}^{-2}$ (see Methods). These results indicate a value of $\alpha = (1.4 \pm 9.1) \times 10^{-5}$, giving the best constraint on the gravitational redshift on the ground. This result is complementary to space tests as it covers the short range (450 m from the surface) in addition to the already covered long range (10^4 km)[10,11] for LPI tests at the 10^{-5} uncertainty level.

In summary, we have developed a pair of compact and accurate optical lattice clocks that can be operated outside laboratories and are capable of centimetre-level chronometric levelling. By transporting the clocks to a broadcasting tower and providing them with a height difference of 450 m, we have tested the gravitational redshift at the 10^{-5} level, which is comparable to recent space experiments. A further constraint on α may be set by improving the clock's uncertainty. By applying a state-of-the-art clock laser[31] and synchronous interrogation of fibre-linked clocks[8], orders of magnitude improvement of the measurement stability will be possible. Such real-time and accurate geopotential measurements at the centimetre level, which are inaccessible by conventional spirit levelling or GNSS height determination, will open up new applications of optical clocks in future geopotentiometry[13] and fundamental physics.

Online content

Any methods, additional references, Nature Research reporting summaries, source data, extended data, supplementary information, acknowledgements, peer review information; details of author contributions and competing interests; and statements of data and code availability are available at https://doi.org/10.1038/s41566-020-0619-8.

Received: 1 October 2019; Accepted: 8 March 2020;
Published online: 6 April 2020

References

1. Nicholson, T. L. et al. Systematic evaluation of an atomic clock at 2×10^{-18} total uncertainty. *Nat. Commun.* **6**, 6896 (2015).
2. Ushijima, I., Takamoto, M., Das, M., Ohkubo, T. & Katori, H. Cryogenic optical lattice clocks. *Nat. Photon.* **9**, 185–189 (2015).
3. McGrew, W. F. et al. Atomic clock performance enabling geodesy below the centimetre level. *Nature* **564**, 87–90 (2018).
4. Brewer, S. M. et al. $^{27}Al^+$ quantum-logic clock with a systematic uncertainty below 10^{-18}. *Phys. Rev. Lett.* **123**, 033201 (2019).
5. Huntemann, N., Sanner, C., Lipphardt, B., Tamm, C. & Peik, E. Single-ion atomic clock with 3×10^{-18} systematic uncertainty. *Phys. Rev. Lett.* **116**, 063001 (2016).
6. Vermeer, M. Chronometric levelling. *Rep. Finnish Geodetic Inst.* **83**, 2 (1983).
7. Pound, R. V. & Snider, J. L. Effect of gravity on gamma radiation. *Phys. Rev.* **140**, B788–B803 (1965).

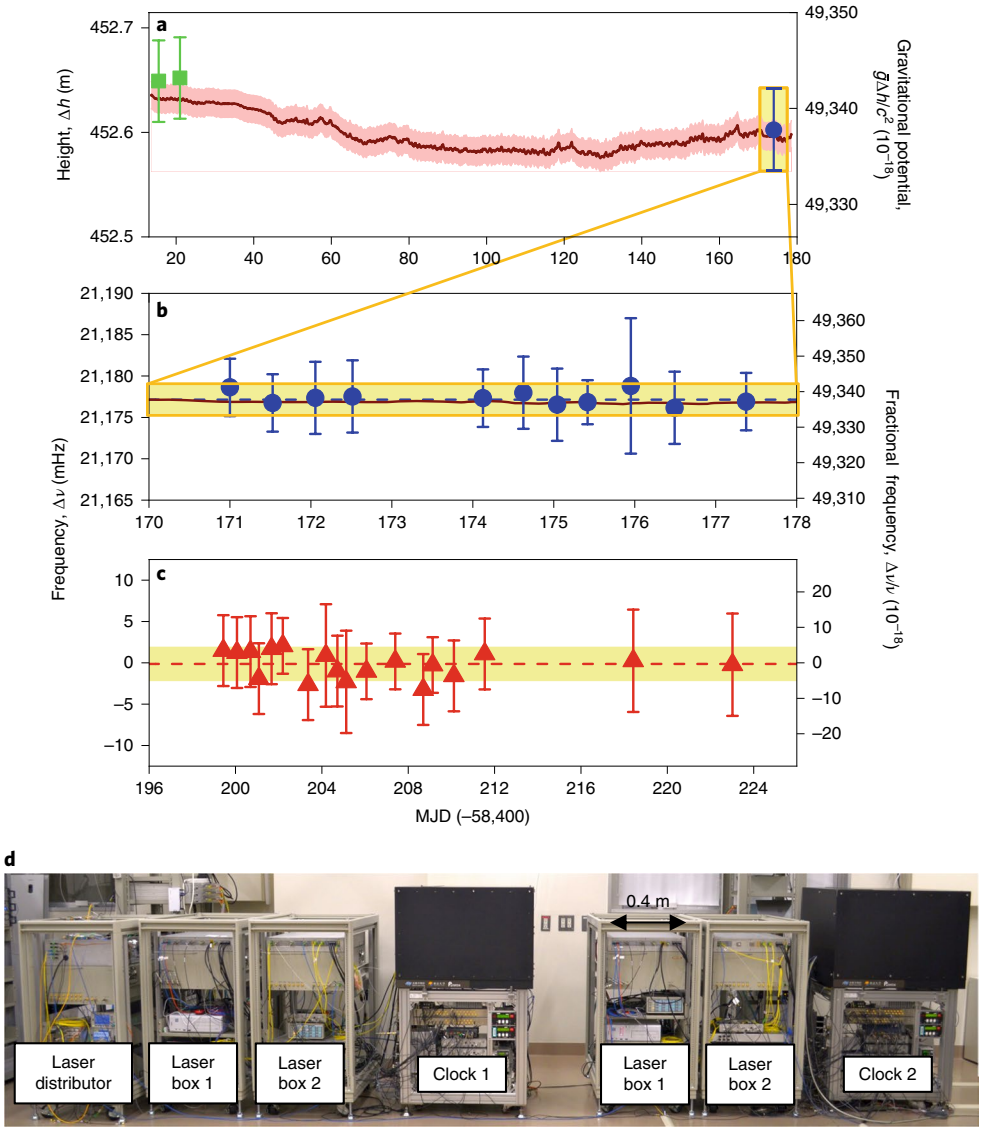

Fig. 3 | Height and frequency differences between two clocks. a, Height differences Δh between the clocks are measured by GNSS (green squares), laser ranging (brown line) and the beat note of the clocks (blue circle) after applying systematic corrections. The continuous laser ranging measures a height variation of ~5 cm that corresponds to the seasonal change in the outer temperature (~10 °C) over six months. The red shaded region shows the uncertainties of height measurements by laser ranging. **b**, The gravitational redshift measured at Skytree (blue circles) is consistent with the gravitational potential difference measured by the laser ranging and gravity measurements (brown line). **c**, The beat note of two clocks set at the same height (red triangles) demonstrates an excellent reproducibility of $(-0.3 \pm 4.7) \times 10^{-18}$. Error bars in **a**–**c** show the square-root sum of the statistical and systematic uncertainties of each measurement. Dashed lines show the average of the clock measurements. Yellow shaded regions show the square-root sum of the statistical and systematic uncertainties of the beat note of the clocks. MJD, modified Julian date. **d**, A pair of clocks tested at the same height. The system operates by providing cooling water, a 24 V power supply and a clock laser, which are not displayed in the photograph.

Table 1 | Summary of height measurements and the frequency difference of two clocks

Measurement period	Height difference Δh (m)		Frequency difference $\Delta\nu/\nu_1$ (10^{-18})	
	GNSS	Laser ranging	450 m–0 m	Same height
MJD 58,414–58,417	452.649(39)	452.632(13)	–	–
MJD 58,420–58,422	452.652(39)	452.631(13)	–	–
MJD 58,571–58,577	–	452.596(13)	49,337.8(4.3)	–
MJD 58,599–58,623	–	–	–	−0.3(4.7)
α parameter	$\alpha = \frac{\Delta\nu}{\nu_1}\frac{c^2}{\bar{g}\Delta h} - 1 = 1.4(9.1) \times 10^{-5}$			

The height differences measured by GNSS and laser ranging are consistent within 2 cm, which is less than the uncertainty of the measurements. Parameter α (equation (1)) is calculated from the gravitational redshift and height difference obtained by laser ranging performed for the same period (MJD 58,571–58,577) with $\bar{g} = 9.797248(24)\,\mathrm{m\,s^{-2}}$. The numbers in parentheses indicate 1σ uncertainties.

8. Takano, T. et al. Geopotential measurements with synchronously linked optical lattice clocks. *Nat. Photon.* **10**, 662–666 (2016).
9. Grotti, J. et al. Geodesy and metrology with a transportable optical clock. *Nat. Phys.* **14**, 437–441 (2018).
10. Delva, P. et al. Gravitational redshift test using eccentric Galileo satellites. *Phys. Rev. Lett.* **121**, 231101 (2018).
11. Herrmann, S. et al. Test of the gravitational redshift with Galileo satellites in an eccentric orbit. *Phys. Rev. Lett.* **121**, 231102 (2018).
12. Bondarescu, R. et al. Ground-based optical atomic clocks as a tool to monitor vertical surface motion. *Geophys. J. Int.* **202**, 1770–1774 (2015).
13. Denker, H. et al. Geodetic methods to determine the relativistic redshift at the level of 10^{-18} in the context of international timescales: a review and practical results. *J. Geodesy* **92**, 487–516 (2017).
14. Lion, G. et al. Determination of a high spatial resolution geopotential model using atomic clock comparisons. *J. Geodesy* **91**, 597–611 (2017).
15. Will, C. M. The confrontation between general relativity and experiment. *Living Rev. Relativ.* **17**, 4 (2014).
16. Brax, P. What makes the universe accelerate? A review on what dark energy could be and how to test it. *Rep. Prog. Phys.* **81**, 016902 (2017).
17. Smarr, L. L., Vessot, R. F. C., Lundquist, C. A., Decher, R. & Piran, T. Gravitational waves and red shifts: a space experiment for testing relativistic gravity using multiple time-correlated radio signals. *Gen. Relativ. Gravit.* **15**, 129–163 (1983).
18. Koller, S. B. et al. Transportable optical lattice clock with 7×10^{-17} uncertainty. *Phys. Rev. Lett.* **118**, 073601 (2017).
19. Cao, J. et al. A compact, transportable single-ion optical clock with 7.8×10^{-17} systematic uncertainty. *Appl. Phys. B* **123**, 112 (2017).
20. Origlia, S. et al. Towards an optical clock for space: compact, high-performance optical lattice clock based on bosonic atoms. *Phys. Rev. A* **98**, 053443 (2018).
21. Sanner, C. et al. Optical clock comparison for Lorentz symmetry testing. *Nature* **567**, 204–208 (2019).
22. Derevianko, A. & Pospelov, M. Hunting for topological dark matter with atomic clocks. *Nat. Phys.* **10**, 933–936 (2014).
23. Stadnik, Y. V. & Flambaum, V. V. Searching for dark matter and variation of fundamental constants with laser and maser interferometry. *Phys. Rev. Lett.* **114**, 161301 (2015).
24. Arvanitaki, A., Huang, J. & Van Tilburg, K. Searching for dilaton dark matter with atomic clocks. *Phys. Rev. D* **91**, 015015 (2015).
25. Van Tilburg, K., Leefer, N., Bougas, L. & Budker, D. Search for ultralight scalar dark matter with atomic spectroscopy. *Phys. Rev. Lett.* **115**, 011802 (2015).
26. Hees, A., Guena, J., Abgrall, M., Bize, S. & Wolf, P. Searching for an oscillating massive scalar field as a dark matter candidate using atomic hyperfine frequency comparisons. *Phys. Rev. Lett.* **117**, 061301 (2016).
27. Wcisło, P. et al. New bounds on dark matter coupling from a global network of optical atomic clocks. *Sci. Adv.* **4**, eaau4869 (2018).
28. Katori, H., Ovsiannikov, V. D., Marmo, S. I. & Palchikov, V. G. Strategies for reducing the light shift in atomic clocks. *Phys. Rev. A* **91**, 052503 (2015).
29. Ushijima, I., Takamoto, M. & Katori, H. Operational magic intensity for Sr optical lattice clocks. *Phys. Rev. Lett.* **121**, 263202 (2018).
30. Takamoto, M., Takano, T. & Katori, H. Frequency comparison of optical lattice clocks beyond the Dick limit. *Nat. Photon.* **5**, 288–292 (2011).
31. Matei, D. G. et al. 1.5 μm lasers with sub-10 mHz linewidth. *Phys. Rev. Lett.* **118**, 263202 (2017).

Methods

Experimental set-up for a one-dimensional optical lattice inside a ring cavity and state preparation in a BBR shield. In the experimental set-up, ^{87}Sr atoms with a nuclear spin of $I=9/2$ are laser-cooled and trapped by a two-stage magneto-optical trap (MOT) sequentially on the $^1S_0(F=9/2)-{}^1P_1(F=11/2)$ and $^1S_0(F=9/2)-{}^3P_1(F=9/2,11/2)$ transitions at 461 nm and 689 nm, respectively[32] (Fig. 1). During the first-stage MOT, atoms relaxed to the $^3P_2$ metastable state are captured by a Green-MOT on the $^3P_2(F=13/2)-(5s5d)^3D_3(F=15/2)$ transition at 496 nm. We use this transition because optical pumping of the hyperfine states to $^3P_2(F=13/2)$ is more efficient than using the $^3P_2-{}^3S_1$ transition at 707 nm. In the Green-MOT, atoms are optically pumped to the $^1S_0$ state or $^3P_0$ state via the $(5s6p)^3P_2$ state, where atoms relaxed to the $^3P_0$ state are optically pumped to either the $^1S_0$ or $^3P_2$ state by a repumping laser on the $^3P_0-(5s6s)^3S_1$ transition at 679 nm, as shown in Supplementary Fig. 2.

Atoms with a temperature of a few μK are loaded into a 1D optical lattice inside a ring cavity. The input power of 22 mW for each counter-propagating lattice laser is enhanced by a factor of ~170, which yields a trap depth of 14 μK ($81E_R$). The atoms in the lattice are transported over 16 mm into a BBR shield by a moving lattice[2], by applying a 60-ms-long frequency chirp to one of the counter-propagating lattice lasers following a cubic polynomial function with a maximum frequency excursion of 1.8 MHz, which is well within the cavity linewidth of ~6 MHz. The relative phase of the counter-propagating lattice lasers is stabilized by detecting the beat note of the lasers transmitted through the cavity and by feeding back to a frequency shifter, as shown in Fig. 1a.

Inside the BBR shield, the atoms are optically pumped to the $^1S_0(F=9/2,m_F=\pm9/2)$ states by a π-polarized laser resonant to the $^1S_0-{}^3P_1(F=7/2)$ transition. The vibrational states of atoms in the axial direction of the lattice are sideband-cooled by a laser resonant to the $^1S_0-{}^3P_1(F=11/2)$ transition[29], which reduces the average vibrational quantum number to $n<0.1$. To select one of the Zeeman substates, $m_F=+9/2$ or $-9/2$, we excite the atoms to the $^3P_0(m_F=+9/2$ or $-9/2)$ state with a 22-ms-long clock π-pulse, which is narrow enough to resolve the spacing of Zeeman substates of ~72 Hz. Atoms in other Zeeman substates are blown away from the lattice by a laser resonant to the $^1S_0-{}^1P_1$ transition. After interrogating the clock transition $^1S_0-{}^3P_0$ at 698 nm, we transport the atoms outside the BBR shield and measure the excited fraction of atoms by laser-induced fluorescence on the $^1S_0-{}^1P_1$ transition. Based on the signal, the frequency shifter is steered to keep the clock laser resonant to the Sr clock transition. The cycle time of the clock interrogation is 1.6 s. We typically average for 10^4 s to achieve 10^{-17} instability (Supplementary Fig. 1b).

Uncertainty budgets for the gravitational redshift measurements. To reduce the systematic uncertainties for the beat note of two clocks, $\Delta\nu=\nu_2-\nu_1$, we operated the two clocks under approximately the same conditions, including the BBR shift, second-order Zeeman shift, lattice and probe light shifts, and collisional shift, to reject some systematics by making them as similar as possible. The corrections and uncertainties for a single clock and beat note measurement are summarized in Supplementary Table 1. The budget for a single clock is represented by that of clock 1, used at 0 m.

BBR shift. The clock transition was interrogated in a well-defined temperature determined by the BBR shield, whose temperature was monitored by two platinum resistance thermometers and stabilized by a four-stage Peltier cooler at 245 K. The thermometers were calibrated within 23 mK. The reproducibility of the controllers was investigated to 2 mK. These uncertainties gave a BBR shift uncertainty of 1.3×10^{-18} for the beat note of the clocks.

The shield has two apertures with diameters of $\phi=1.00(5)$ mm to introduce the atoms and lasers. Consequently, the interrogated atoms are exposed to the external room-temperature environment at $T_{ext}=298(5)$ K with a solid angle of $\Omega=19(4)$ msr, which give a BBR shift uncertainty of 1.4×10^{-18}. The inner wall of the BBR shield is black-coated with Ultra Black (provided by Acktar) to reduce the multiple reflections of room-temperature BBR[2]. Applying a Monte Carlo ray-tracing simulation, the BBR shift induced by the multiple reflections gives an uncertainty of 1.6×10^{-19} for the black-coated inner wall with an emissivity of 0.9. The uncertainty of the BBR shift due to the atom loading position was calculated to be 2.7×10^{-19} for a position uncertainty of ±1 mm, provided by the uncertainty of the initial lattice loading position for the MOT. The overall BBR uncertainty was evaluated as the square-root-sum of these four contributions.

Zeeman shift. A bias magnetic field of 66 μT was applied to define the quantization axis for clock spectroscopy. The magnetic field was stable within 0.03 μT over the measurement period of one week thanks to a μ-metal shield surrounding the physics package. The first-order Zeeman shift and the vector light shift were cancelled out[33] by averaging two Zeeman components of the clock transition frequencies $\nu_\pm$ that correspond to the $^1S_0(m_F=\pm9/2)$ and $^3P_0(m_F=\pm9/2)$ states. The first-order Zeeman shift of $\nu_+-\nu_-\approx651$ Hz was continuously monitored. By applying the same bias magnetic field (agreeing within 66 ppm for the two clocks), the second-order Zeeman shift of $\sim-2.424(3)\times10^{-16}$ was mostly rejected and a correction as small as $-3.28(4)\times10^{-20}$ remained in the redshift measurements.

Lattice light shift. We applied the operational magic condition for Sr[28,29] by tuning the lattice laser to $\nu_L=368{,}554{,}470.4(2)$ MHz with a trap depth $81E_R$. The residual light shift was estimated to be $1.1(6)\times10^{-18}$ (the finite vibrational quantum number of $n=0.06(2)$ causes major uncertainty). The lattice laser was linearly polarized with an extinction ratio of >40 dB. Its polarization vector $\boldsymbol{\epsilon}_L$ and the quantization axis given by the bias magnetic field $\mathbf{e}_B=\mathbf{B}_{bias}/|\mathbf{B}_{bias}|$ were aligned to be parallel by controlling the magnetic field with three pairs of Helmholtz coils. The uncertainty of the angle $\theta=\cos^{-1}(\boldsymbol{\epsilon}_L\cdot\mathbf{e}_B)$ was estimated to be less than 23 mrad, which corresponds to an uncertainty of the tensor light shift of 0.5×10^{-18}. A tapered amplifier was used for the lattice, where the amplified spontaneous emission (ASE), which is 40 dB below the carrier spectrum with a resolution bandwidth of 1 nm, was spectrally filtered by a volume Bragg grating (VBG) with a bandwidth of 35 pm. The light shift estimated by the ASE spectrum and the filtering characteristic of VBG was less than 10^{-19}.

Probe light shift. The probe light shift was determined with an uncertainty of 5%. The intensity of the clock laser was determined with an uncertainty of 2.7% by comparing the observed Ramsey fringes and the calculated spectra. As we applied a similar clock laser intensity for two clocks, the probe light shift mostly cancelled in the redshift measurement and gave a probe light shift uncertainty of 2.8×10^{-18} (given by the uncertainty of the clock laser intensity).

Density shift. We designed the $1/e^2$ diameter of the lattice laser to be 330 μm to keep the atomic density relatively low. Assuming the density shift $\kappa_i N_i$ to be proportional to the number of trapped atoms N_i located at $i=1,2$, the clock frequency difference $\Delta\nu_d$, including the density shift, is given by $\Delta\nu_d=\Delta\nu+(\kappa_2N_2-\kappa_1N_1)$, where $\Delta\nu$ is the gravitational redshift. We obtained $\Delta\nu$ by fitting the frequency difference $\Delta\nu_d$ with variables N_1 and N_2, and free parameters $\Delta\nu$, κ_1 and κ_2. The density shift of a low 10^{-18} is included in Fig. 3, where we apply coefficients of $\kappa_1=0.08(33)$ μHz per atom and $\kappa_2=-1.49(30)$ μHz per atom, obtained from the fitting. We typically interrogated $N\approx1{,}500$ atoms.

First-order Doppler shift. Doppler noise cancellers were installed for the lattice and clock lasers by sharing a partial reflector as a reference surface (Fig. 1a), where the path length of $L_1\approx10$ mm between mirror M4 and the partial reflector remained uncompensated. There was another uncompensated path of $L_2\approx300$ mm for the clock laser. These introduced uncertainties in the first-order Doppler shift of 0.8×10^{-19} and 5.3×10^{-19}, respectively, assuming a diurnal temperature variation of 10 K for L_1 in a room-temperature environment and 2 K for L_2 on a water-cooled breadboard.

Other contributions. Servo error was evaluated by averaging the imbalance of the excitation fraction at a detuning of $\pm\gamma/2$ from the centre of the Ramsey fringe, where $\gamma\approx9$ Hz is the linewidth of the spectrum with a free evolution time of 40 ms. The resultant frequency shifts of $0.0(2)\times10^{-18}$ and $0.1(2)\times10^{-18}$ at 0 m and 450 m, respectively, are corrected in Fig. 3b,c.

Background gas collision was estimated to be $-5.4(1.0)\times10^{-18}$ based on ref. [34], assuming that the observed lifetime of 5.6(9) s is limited by collisional loss with H_2 molecules. In the redshift measurement, the collisional shift was mostly rejected and its uncertainty is given by that of lifetime measurements.

Evaluation of gravitational potential difference by measuring gravity and height difference. In parallel with the chronometric levelling, the gravitational potential difference between the two clocks was investigated by laser ranging and GNSS, complemented by spirit levelling and a gravimeter. Supplementary Table 2 summarizes the height measurements performed during MJD periods 58,414–58,417 and 58,420–58,422. Averaging the five-day-long height data of the two clocks measured with GNSS results in 452.650(39) m, with the uncertainty dominated by the statistics of the GNSS data. Measurement based on laser ranging in the same period gives 452.631(13) m, which agrees with the GNSS measurement within 1σ uncertainty.

The clock comparison was performed during the period MJD 58,571–58,577. The laser ranging continuously monitored the height difference between the clocks from October 2018 to April 2019 to find the seasonal variation of height $\Delta h\approx5$ cm due to the temperature change, as shown in Fig. 3a.

Laser ranging. We continuously measured the height in four separate sections (0–150 m, 150–250 m, 250–370 m and 385–445 m), which covers ~94% (~427 m) of the total height, using four commercial laser distance meters (LDM51, Jenoptik). Each measurement gave a height uncertainty of 4.7 mm, including the systematic uncertainty of the instruments and statistical uncertainty. The obtained data were corrected by monitoring the onsite temperature, humidity and pressure, giving a height uncertainty of 2 mm. By including a short height measurement (~4 m), we estimated the overall uncertainty of the laser ranging to be 10 mm.

Spirit levelling. The height of the remaining part (~20 m) was measured by spirit levelling on MJD 58,382, 58,414 and 58,417. The spirit levelling was conducted with ZEISS Dini0.3 (instrument) and LD12 (rods), and the total uncertainty of

the levelling was 2 mm. By including the miscellaneous heights of 0.575 m from the setting of the instruments measured with a ruler and the thickness of the floor measured with a radar, the total uncertainty of the height measurement for laser ranging and spirit levelling was 13 mm.

GNSS measurement. Height measurements using GNSS were performed in October 2018 during MJD periods 58,414–58,417 and 58,420–58,422. As shown in Fig. 2a, one of the GNSS antennas (ChokeRing TMR29659.00, Trimble) was located at the 458 m floor and the other was set on the ground, ~700 m away from Tokyo Skytree, where calm conditions were maintained during measurements. GPS and GLONASS were monitored by GNSS receivers (Trimble R7 GNSS) with 1 Hz sampling during each period and were processed by the post kinematic method with the final orbit of the International GNSS Service (IGS) using RTKLIB software[35]. The fix rates were 99.5% and 94.7% during the first and second period, respectively. To verify the difference in ellipsoidal and orthometric height between Tokyo Skytree and the ground GNSS antennas, another GNSS measurement was conducted at the foot of the tower for 6 h on MJD 58,414. The data were processed by the static method with the IGS final orbit using GAMIT/GLOBK software[36]. The height between the clocks and the GNSS antennas (~8 m) was measured by spirit levelling. The uncertainty of the height measurement obtained by GNSS and spirit levelling was 39 mm.

Gravitational acceleration measurement. The gravitational acceleration at the locations of the clocks in Tokyo Skytree was measured on MJD 58,415 with relative gravimeters, a LaCoste & Romberg gravimeter (Model G) and a Scintrex CG-5 Autograv gravimeter. Both gravimeters are calibrated annually and show consistent gravity values with uncertainties of 0.02 mGal. The results are connected to the absolute gravity value at a reference point in Tsukuba, which is part of the Japan Gravity Standardization Net 2016[37]. To obtain the baseline gravity values between the location of the clocks and the reference point, we adopted various corrections to the measurement data such as the effect of solid-earth tide, ocean tide and atmospheric pressure. The gravitational acceleration in Tokyo Skytree was measured to be $g_0 = 9.7979441\,\mathrm{m\,s^{-2}}$ at 0 m and $g_{450} = 9.7965514\,\mathrm{m\,s^{-2}}$ at 450 m. The averaged gravitational acceleration was determined to be $\bar{g} = \frac{g_0 + g_{450}}{2} = 9.797248(24)\,\mathrm{m\,s^{-2}}$. In the analysis of gravitational potential difference, the higher-order terms of the height dependence of gravitational acceleration contribute to α as small as 1.2×10^{-9}. The measurement uncertainty of $\delta\bar{g} = 2.4\,\mathrm{mGal}\ (= 2.4 \times 10^{-5}\,\mathrm{m\,s^{-2}})$, which corresponds to $\frac{\delta\bar{g}\Delta h}{c^2} \approx 1 \times 10^{-19}$, is dominated by fluctuation of the gravity values measured at 450 m in Tokyo Skytree due to vibrations of the tower. Seasonal and long-term changes in gravity are typically less than 0.01 mGal and 0.01 mGal per year, both of which are much smaller than the measurement uncertainty. The mass of Tokyo Skytree affects the gravity measurement at 0 m and 450 m by 0.1 mGal, which is much smaller than the measurement uncertainty.

Data availability

All data obtained in the study are available from the corresponding author upon reasonable request.

References

32. Mukaiyama, T., Katori, H., Ido, T., Li, Y. & Kuwata-Gonokami, M. Recoil-limited laser cooling of ^{87}Sr atoms near the Fermi temperature. *Phys. Rev. Lett.* **90**, 113002 (2003).
33. Takamoto, M. et al. Improved frequency measurement of a one-dimensional optical lattice clock with a spin-polarized fermionic ^{87}Sr isotope. *J. Phys. Soc. Jpn* **75**, 104302 (2006).
34. Alves, B. X. R., Foucault, Y., Vallet, G. & Lodewyck, J. Background gas collision frequency shift on lattice-trapped strontium atoms. In *2019 Joint Conference of the IEEE International Frequency Control Symposium and European Frequency and Time Forum* (IEEE, 2019).
35. Takasu, T. *RTKLIB: An Open Source Program Package for GNSS Positioning* (RTKLIB, accessed 8 July 2019); http://www.rtklib.com/rtklib.htm
36. King, R. W. & Bock, Y. *Documentation for the GAMIT GPS Analysis Software* (MIT, 2004).
37. Yahagi, T., Yoshida, K., Miyazaki, T., Hiraoka, Y. & Miyahara, B. Construction of the Japan Gravity Standardization Net 2016. *Bull. Geospatial Information Authority of Japan* **66**, 49–58 (2018).

Acknowledgements

This work received support from a Japan Society for the Promotion of Science (JSPS) Grant-in-Aid for Specially Promoted Research (grant no. JP16H06284) and Japan Science and Technology Agency (JST)-Mirai Program grant no. JPMJMI18A1. H.S. acknowledges support from JSPS KAKENHI grant no. JP17H06358. We thank Shimadzu Corporation for development of control electronics for the laser system, Geospatial Information Authority of Japan for GNSS, levelling and gravity measurements, Tobu Tower Skytree Co. for support of the experiments, J. Fortágh and L. Sárkány for the loan of wavelength meters, Y. Takahashi from Citizen Watch Co. for development of a laser system, M. Kokubun for support with electronics, K. Araki for designing control electronics, T. Takahashi, H. Ichikawa and A. Gomyo for laser ranging measurements and A. Hinton for reading the manuscript.

Author contributions

H.K. envisaged and initiated the experiments. H.K., M.T., I.U. and N.O. designed the apparatus and experiments. I.U., M.T. and N.O. carried out experiments and analysed data. T.Y. and K.K. conducted geodetic measurements. All authors discussed the results and contributed to the writing of the draft.

Competing interests

The authors declare no competing interests.

Additional information

Supplementary information is available for this paper at https://doi.org/10.1038/s41566-020-0619-8.

Correspondence and requests for materials should be addressed to H.K.

Terms and Conditions

Springer Nature journal content, brought to you courtesy of Springer Nature Customer Service Center GmbH (“Springer Nature”).
Springer Nature supports a reasonable amount of sharing of research papers by authors, subscribers and authorised users (“Users”), for small-scale personal, non-commercial use provided that all copyright, trade and service marks and other proprietary notices are maintained. By accessing, sharing, receiving or otherwise using the Springer Nature journal content you agree to these terms of use (“Terms”). For these purposes, Springer Nature considers academic use (by researchers and students) to be non-commercial.
These Terms are supplementary and will apply in addition to any applicable website terms and conditions, a relevant site licence or a personal subscription. These Terms will prevail over any conflict or ambiguity with regards to the relevant terms, a site licence or a personal subscription (to the extent of the conflict or ambiguity only). For Creative Commons-licensed articles, the terms of the Creative Commons license used will apply.
We collect and use personal data to provide access to the Springer Nature journal content. We may also use these personal data internally within ResearchGate and Springer Nature and as agreed share it, in an anonymised way, for purposes of tracking, analysis and reporting. We will not otherwise disclose your personal data outside the ResearchGate or the Springer Nature group of companies unless we have your permission as detailed in the Privacy Policy.
While Users may use the Springer Nature journal content for small scale, personal non-commercial use, it is important to note that Users may not:

1. use such content for the purpose of providing other users with access on a regular or large scale basis or as a means to circumvent access control;
2. use such content where to do so would be considered a criminal or statutory offence in any jurisdiction, or gives rise to civil liability, or is otherwise unlawful;
3. falsely or misleadingly imply or suggest endorsement, approval , sponsorship, or association unless explicitly agreed to by Springer Nature in writing;
4. use bots or other automated methods to access the content or redirect messages
5. override any security feature or exclusionary protocol; or
6. share the content in order to create substitute for Springer Nature products or services or a systematic database of Springer Nature journal content.

In line with the restriction against commercial use, Springer Nature does not permit the creation of a product or service that creates revenue, royalties, rent or income from our content or its inclusion as part of a paid for service or for other commercial gain. Springer Nature journal content cannot be used for inter-library loans and librarians may not upload Springer Nature journal content on a large scale into their, or any other, institutional repository.
These terms of use are reviewed regularly and may be amended at any time. Springer Nature is not obligated to publish any information or content on this website and may remove it or features or functionality at our sole discretion, at any time with or without notice. Springer Nature may revoke this licence to you at any time and remove access to any copies of the Springer Nature journal content which have been saved.
To the fullest extent permitted by law, Springer Nature makes no warranties, representations or guarantees to Users, either express or implied with respect to the Springer nature journal content and all parties disclaim and waive any implied warranties or warranties imposed by law, including merchantability or fitness for any particular purpose.
Please note that these rights do not automatically extend to content, data or other material published by Springer Nature that may be licensed from third parties.
If you would like to use or distribute our Springer Nature journal content to a wider audience or on a regular basis or in any other manner not expressly permitted by these Terms, please contact Springer Nature at

onlineservice@springernature.com